Decentralized PID Control of Magnetic Bearings in a Rotor System

An-Chen Lee
Professor

Yi-Hua Fan
Research Assistant

Dept. of Mechanical Engineering, National Chiao Tung University
1001 Ta Hsueh Road, Hsinchu 300, Taiwan, R. O. C.
Fax: 886-35-725372, E-mail: aclee@cc.nctu.edu.tw

Abstract

The decentralized PID controller design for a permanent/electromagnetic magnetic bearing (PEMB) system that suspends a high-speed rigid horizontal rotor is investigated in this paper. Two types of decentralized PID controllers are proposed. Considering the gyroscopic effect, a design procedure is presented. Simulation results show that the larger the ratio of polar mass moment of inertia to transverse mass moment of inertia in a rotor, the more significant the gyroscopic effect will affect the system stability. To facilitate implementation, we developed a controller together with bipolar linear current amplifiers for the PEMBs. Experiments show that the rotor's whirling orbits can be maintained within an acceptable small range (30 μm) when the rotor operates in the speed range from 0 to 12,000 rpm.

1. Introduction

Magnetic bearings can suspend a rotating shaft by attractive magnetic force without mechanical contact and lubrication. The major advantages of these bearings are that they eliminate traditional bearing problems such as wear and lubrication and, even more important, offer great potential for vibration reduction. However, the attractive magnetic suspension system used in magnetic bearings is inherently unstable; thus, artificial stabilization by means of feedback control is required. There is much literature concerning with the control strategy in magnetic bearing rotor systems. Most of them [1~4] emphasized on the central control; thus the feedback control algorithms become very complicated because each control input depends on all degrees of freedom of the rotor. On the other hand, some researchers have investigated the decentralized control [5~7] of magnetic bearing rotor systems and proposed the geometry condition for decentralization. However, most of them designed the decentralized controller without considering the gyroscopic effect on the system stability as the rotating speed increases.

In this paper, we propose two types of decentralized controllers for a rigid symmetrical rotor supported by PEMBs. Two kinds of rotor systems (i.e., long rotor and short rotor) are adopted to study the gyroscopic effect on system stability. Simulation results show that the closed-loop stability for a long rotor system can be guaranteed as the operating speed up to 945,000 rpm; however, for a short rotor, it can only be operated up to 7,050 rpm. Experiment for the long rotor system is conducted and the results show that the rotor's whirling orbits can be maintained within 30 μm by the proposed controller when the rotor operates at the speed from 0 to 12,000 rpm.

2. Modeling the Horizontal Rotor-Bearing System

Fig. 1 shows the basic structure of the attractive type magnetic bearing rotor system. The rotor is suspended by two sets of PEMBs together with a motor to drive the rotor. The shaft is suspended horizontally by contact-free magnetic bearings at both sides and the rotor positions are measured by four eddy-current-type sensors at the magnetic-bearing location. Furthermore, the rotor is assumed to be rigid and symmetric with uniform mass unbalance, and have small displacements from the desired position. The attractive forces provided by the electromagnets acting on the rotor are expressed as F_n (n=1,..,8). Fig. 1 also shows the direction and point of action of each displacement and force.

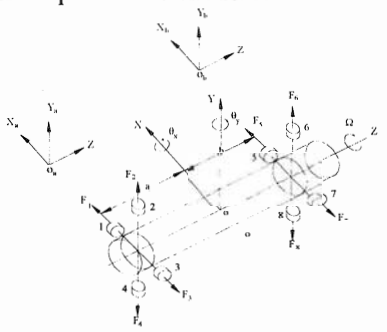

Fig. 1 Basic structure of the rotor-bearing system

The dynamic equations of the rotor bearing system about the mass center can be expressed as follows:

$$\begin{aligned} m\ddot{x} &= m(\varepsilon\Omega^2\cos\Omega t - \eta\Omega^2\sin\Omega t) + F_1 - F_3 + F_5 - F_7 \\ m\ddot{y} &= m(\varepsilon\Omega^2\sin\Omega t + \eta\Omega^2\cos\Omega t) - mg + F_2 - F_4 + F_6 - F_8 \\ I_r\ddot{\theta}_y - I_p\Omega\dot{\theta}_x &= \frac{L}{2}(-F_1 + F_3 - F_5 + F_7) \\ I_r\ddot{\theta}_x + I_p\Omega\dot{\theta}_y &= \frac{L}{2}(F_2 - F_4 + F_6 - F_8) \end{aligned} \quad (1)$$

where Ω is the rotational speed about the spinning Z axis, m is the rotor mass, I_r and I_p are the transverse and polar mass moment of inertia of the rotor, respectively; ε and η are the mass eccentricity components of the rotor corresponding to the X- and Y- axes, respectively.

From our previous studies [8,9], the magnetic forces F_1 to F_8 provided by the two sets of PEMBs are functions of the length of the air gap and the magnitude of the magnetic flux, which is the sum of the electromagnet (EM) flux and permanent magnet (PM) bias flux. The length of the air gap is dependent upon the nominal length of the gap and

the rotor displacement from the center position of the magnetic bearing. Because the EM flux due to the coil current is far less than the PM bias flux and the rotor displacement is confined to one-tenth the gap length under normal operation, the magnetic force may be approximated by a Taylor expansion about the normal operating point $i_n=0$ and $d_n=0$, by taking only those terms less than second order into consideration, i.e., the magnetic force can be expressed as:

$$F_n=f_0+k_d d_n+k_i i_n \tag{2}$$

where f_0 is the static magnetic force when $i_n=0$ and $d_n=0$; k_d and k_i is the force-displacement stiffness and the force-current stiffness, respectively; and the eight electromagnets have same values of k_d and k_i.

Furthermore, the currents flowing through the electromagnets in our design, as shown in figure 2, are assigned as:

$$i_1=-i_3,\ i_2=-i_4,\ i_5=-i_7,\ i_6=-i_8. \tag{3}$$

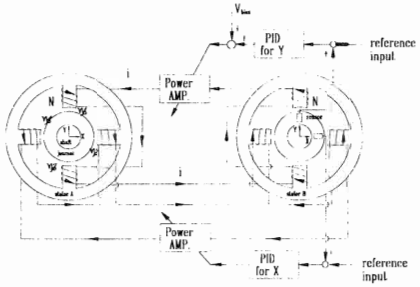

Fig. 2 Control circuit for a permanent-magnet biased magnetic bearing

To simplify the controller design, we will express the system equations in terms of displacements at the magnetic-bearing locations. Since the rotor is assumed to be rigid and the displacement from the desired position is assumed to be small, the relationships between x_a, x_b,, y_a and y_b and x, y, θ_x and θ_y can be expressed as follows:

$$x=\frac{bx_a+ax_b}{L} \qquad y=\frac{by_a+ay_b}{L}$$

$$\theta_x\cong\tan\theta_x=\frac{y_a-y_b}{L} \qquad \theta_y\cong\tan\theta_y=\frac{x_b-x_a}{L} \tag{4}$$

Substituting equations (2-4) into equation (1) yields the dynamics of the system in terms of displacements at the magnetic-bearing locations, which can be rearranged in matrix form as follows:

$$M\ddot{\underline{x}}+C\dot{\underline{x}}+K\underline{x}=B\underline{u}+E\underline{w}+Dg \tag{5}$$

where

$$M=I_{4x4}$$

$$C=\begin{bmatrix} 0 & 0 & \alpha_1 & -\alpha_1 \\ 0 & 0 & -\alpha_2 & \alpha_2 \\ -\alpha_1 & \alpha_1 & 0 & 0 \\ \alpha_2 & -\alpha_2 & 0 & 0 \end{bmatrix}$$

$$K=-\begin{bmatrix} \beta_1+a^2\beta_2 & \beta_1-ab\beta_2 & 0 & 0 \\ \beta_1-ab\beta_2 & \beta_1+b^2\beta_2 & 0 & 0 \\ 0 & 0 & \beta_1+a^2\beta_2 & \beta_1-ab\beta_2 \\ 0 & 0 & \beta_1-ab\beta_2 & \beta_1+b^2\beta_2 \end{bmatrix}$$

$$B=\begin{bmatrix} \gamma_1+a^2\gamma_2 & \gamma_1-ab\gamma_2 & 0 & 0 \\ \gamma_1-ab\gamma_2 & \gamma_1+b^2\gamma_2 & 0 & 0 \\ 0 & 0 & \gamma_1+a^2\gamma_2 & \gamma_1-ab\gamma_2 \\ 0 & 0 & \gamma_1-ab\gamma_2 & \gamma_1+b^2\gamma_2 \end{bmatrix}$$

$$E=\begin{bmatrix} \varepsilon & -\eta \\ \varepsilon & -\eta \\ \eta & \varepsilon \\ \eta & \varepsilon \end{bmatrix} \qquad D=\begin{bmatrix} 0 \\ 0 \\ -1 \\ -1 \end{bmatrix}$$

$$\underline{x}=\begin{bmatrix} x_a & x_b & y_a & y_b \end{bmatrix}^T \qquad \underline{u}=\begin{bmatrix} i_1 & i_5 & i_2 & i_6 \end{bmatrix}^T$$

$$\underline{w}=\begin{bmatrix} \Omega^2\cos\Omega t & \Omega^2\sin\Omega t \end{bmatrix}^T$$

$$\alpha_1=\frac{\Omega I_p a}{I_r L} \qquad \beta_1=\frac{2k_d}{m} \qquad \gamma_1=\frac{2k_i}{m}$$

$$\alpha_2=\frac{\Omega I_p b}{I_r L} \qquad \beta_2=\frac{2k_d}{I_r} \qquad \gamma_2=\frac{2k_i}{I_r}$$

3. Controller Design

First, we try to eliminate the effect of weight by separating the coil current i_j, j=1~8, into two parts: one is the static part i_{j0} to provide a static force, and the other is the dynamic part i_j^* (i.e., the controlled current) to provide a dynamic force. Thus, we can represent the incremental current as

$$i_j=i_j^*+i_{j0} \qquad j=1,\cdots,8 \tag{6}$$

Furthermore, to ensure these static forces not to induce any initial torque, we have the following relationships:

$$i_{20}=-i_{40}=\frac{bmg}{2(a+b)k_i}, \qquad i_{60}=-i_{80}=\frac{amg}{2(a+b)k_i},$$

$$i_{10}=i_{30}=i_{50}=i_{70}=0. \tag{7}$$

As shown in Fig. 3, the control system controls the positions of the rotor by providing current to the electromagnet according to the signals from the position sensors. The distances between the magnet poles and the shaft are measured by eddy-current-type position sensors. Signals from the position sensors are then compared with the reference signals, which correspond to the rotor's central position.

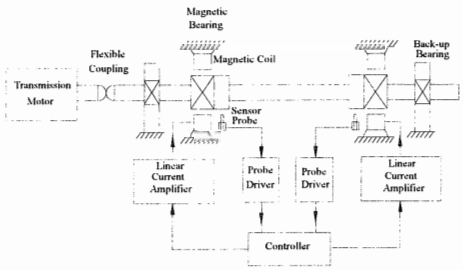

Fig. 3 Schematic diagram of the control system

The error signals measured from two magnetic bearings are proportional to the difference between the central position and the actual position of the rotor at any given time. If both error signals are zero, the rotor position is in the center of the stator. In response to the magnitude of the error signals, the controller generates a suitable low power voltage signal to drive the power amplifier and then the power amplifier provides the control currents to the

winding coils so that suitable bearing forces are generated and the desired rotor position is maintained.

Furthermore, since the time constant of the sensor and driver are normally very small, we can neglect the delay phenomenon. The dynamic equations of the sensor and driver can be expressed as

$$V_c(j)=g_s\underline{x}(j), \quad j=1,2,3,4 \tag{8}$$

and

$$\underline{u}^*(j)=g_d V_c(j), \quad j=1,2,3,4 \tag{9}$$

where $V_c(j)$ is the error signal in voltage, which is the difference between the measured voltage of the sensor and the reference input; $V_c(j)$ is the output voltage generated by the controller; g_s and g_d are the constant gain of the sensor and driver, respectively; and $\underline{x}(j)$ represents the rotor displacements at the magnetic-bearing locations; $\underline{u}^*=[i_1^*\ i_5^*\ i_2^*\ i_6^*]^T$ is the control input consisting of the dynamic part of coil currents.

The PID control law can then be expressed as

$$V_c(j)=-K_pV_c(j)-K_d\dot{V}_c(j)-K_i\int V_c(j)dt \tag{10}$$

where K_p, K_d and K_i are the position, velocity and integral feedback gain matrices, respectively.

Thus, the overall dynamics of the system is:

$$M\ddot{\underline{x}}+C\dot{\underline{x}}+4k_ig_sg_dK_d\dot{\underline{x}}+(K+4k_ig_sg_dK_p)\underline{x}+4k_ig_sg_dK_i\int\underline{x}dt=E\underline{w} \tag{11}$$

From the previous study [7], if we set $a=b=L/2$, define $K_p=B^{-1}K_p^*$, $K_d=B^{-1}K_d^*$ and $K_i=B^{-1}K_i^*$, and choose

$$K_p^*=diag(\kappa_p^*, \kappa_p^*, \kappa_p^*, \kappa_p^*) \tag{12}$$

$$K_d^*=diag(\kappa_d^*, \kappa_d^*, \kappa_d^*, \kappa_d^*) \tag{13}$$

$$K_i^*=diag(\kappa_i^*, \kappa_i^*, \kappa_i^*, \kappa_i^*), \tag{14}$$

the four subsystems will have the same dynamics. Under these circumstances, we have $\alpha_1=\alpha_2$, and

$$C=G_c=\begin{bmatrix} 0 & 0 & \alpha & -\alpha \\ 0 & 0 & -\alpha & \alpha \\ -\alpha & \alpha & 0 & 0 \\ \alpha & -\alpha & 0 & 0 \end{bmatrix}, \quad \alpha=\frac{I_p\Omega}{2I_r}.$$

Then, the control law can be expressed as:

$$\begin{bmatrix} i_1^* \\ i_5^* \end{bmatrix}=-B_1\left(\begin{bmatrix} \kappa_p & 0 \\ 0 & \kappa_p \end{bmatrix}\begin{bmatrix} x_a \\ x_b \end{bmatrix}+\begin{bmatrix} \kappa_d & 0 \\ 0 & \kappa_d \end{bmatrix}\begin{bmatrix} \dot{x}_a \\ \dot{x}_b \end{bmatrix}+\begin{bmatrix} \kappa_i & 0 \\ 0 & \kappa_i \end{bmatrix}\begin{bmatrix} \int x_a dt \\ \int x_b dt \end{bmatrix}\right)$$

$$\begin{bmatrix} i_2^* \\ i_6^* \end{bmatrix}=-B_1\left(\begin{bmatrix} \kappa_p & 0 \\ 0 & \kappa_p \end{bmatrix}\begin{bmatrix} y_a \\ y_b \end{bmatrix}+\begin{bmatrix} \kappa_d & 0 \\ 0 & \kappa_d \end{bmatrix}\begin{bmatrix} \dot{y}_a \\ \dot{y}_b \end{bmatrix}+\begin{bmatrix} \kappa_i & 0 \\ 0 & \kappa_i \end{bmatrix}\begin{bmatrix} \int y_a dt \\ \int y_b dt \end{bmatrix}\right) \tag{15}$$

where $B_1=\frac{g_sg_d}{L^2\gamma_1\gamma_2}\begin{bmatrix} \gamma_1+L^2\gamma_2/4 & -\gamma_1+L^2\gamma_2/4 \\ -\gamma_1+L^2\gamma_2/4 & \gamma_1+L^2\gamma_2/4 \end{bmatrix}$

Finally, the overall system characteristic equation is:

$$\left\{\left[s^3+4k_ig_sg_d\kappa_ds^2+(4k_ig_sg_d\kappa_p/m-L^2k_d/I_r)s+4k_ig_sg_d\kappa_i/m\right]^2+4\times\left(I_p\Omega/2I_r\right)^2s^4\right\}\times\left[s^3+4k_ig_sg_d\kappa_ds^2+(4k_ig_sg_d\kappa_p/m-4k_d/m)s+4k_ig_sg_d\kappa_i/m\right]^2=0 \tag{16}$$

Thus, by neglecting the gyroscopic effect, the stability condition for each subsystem can be determined by Routh's stability criterion:

$$\kappa_p>\max\left\{\frac{k_d}{g_sg_dk_i}, \frac{k_d}{g_sg_dk_i}\right\}$$

$$\kappa_d>0$$

$$0\le\kappa_i\le\min\left\{\frac{(4k_ig_sg_d\kappa_p-4k_d)\times\kappa_d}{m}, \frac{(4k_ig_sg_d\kappa_p-mL^2k_d/I_r)\times\kappa_d}{m}\right\} \tag{17}$$

Obviously, the four pairs of electromagnets can be implemented independently without horizontal and vertical interaction. We call such a system as a semi-decentralized controller. Figure 4 is the block diagram of the overall system for the semi-decentralized case.

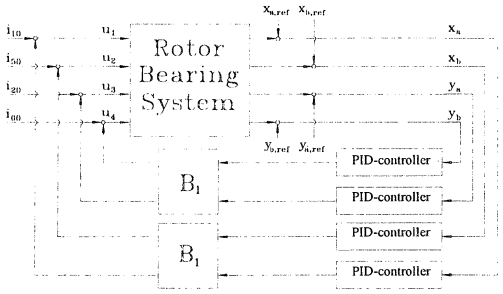

Fig. 4 Block diagram of the semi-decentralized controlled system

Furthermore, let $a=b=L/2$, and $4I_r/L^2=m$, then we have $B=4k_i/mI_{4\times4}$, and $K=-4k_d/mI_{4\times4}$, and the equations of motion (5) can be simplified as follows:

$$I\ddot{\underline{x}}+G_c\dot{\underline{x}}-\frac{4k_d}{m}I\underline{x}=\frac{4k_i}{m}I\underline{u}^*+E\underline{w} \tag{18}$$

where I is a 4x4 identity matrix.

Set K_p, K_d and K_i to be diagonal matrices and have the same control gains, expressed as follows:

$$K_p=diag(\kappa_p, \kappa_p, \kappa_p, \kappa_p) \tag{19}$$

$$K_d=diag(\kappa_d, \kappa_d, \kappa_d, \kappa_d) \tag{20}$$

$$K_i=diag(\kappa_i, \kappa_i, \kappa_i, \kappa_i). \tag{21}$$

We can obtain the decentralized PID control system. Figure 5 shows the block diagram of such control system.

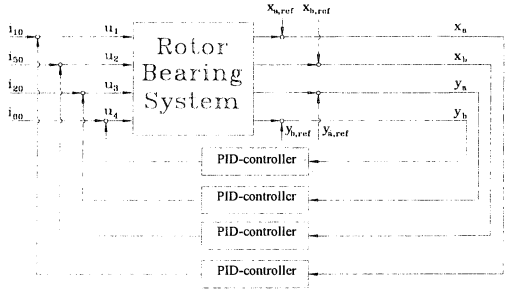

Fig. 5 Block diagram of the decentralized PID control system

The overall system characteristic equation is

$$\left\{\left[s^3+4k_ig_sg_d\kappa_ds^2+(4k_ig_sg_d\kappa_p-4k_d)s+4k_ig_sg_d\kappa_i\right]^2+4\times\left(I_p\Omega/2I_r\right)^2s^4\right\}\times\left[s^3+4k_ig_sg_d\kappa_ds^2+(4k_ig_sg_d\kappa_p-4k_d)s+4k_ig_sg_d\kappa_i\right]^2=0 \tag{22}$$

Neglecting the gyroscopic effect, the stability condition can be derived as:

$$\kappa_p>\frac{k_d}{g_sg_dk_i}$$

$$\kappa_d>0$$

$$0 \le \kappa_i \le \frac{(4k_i g_s g_d \kappa_p - 4k_d) \times \kappa_d}{m} \quad (23)$$

The decentralized PID controller is often designed by neglecting the gyroscopic effect [5]. However, examining equations 16 and 22, we found that the gyroscopic effect in both cases would appear in the fourth term of the first parentheses. As the rotating speed increases, the system will tend to be unstable, obviously. Thus, neglecting the gyroscopic effect in designing the semi-decentralized or decentralized PID controller is not always suitable for all rotor system.

To further explore this effect, two kinds of rotor system are adopted, i.e., a long shaft system, such as a spindle, and a short shaft system, such as a turbine or a flying wheel. Basic structures are shown in Figure 6. The decentralized PID controlled system is employed in both cases.

(a) Long rotor

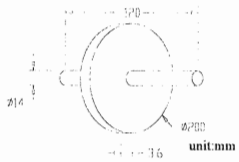

(b) Short rotor

Fig. 6 Basic structures of rotors

The two systems are suspended by the same magnetic bearing and controlled by decentralized PID structure with the same feedback gain, assigned to be κ_p=2.35, κ_i=65 and κ_d=0.01. Thus, both systems have the same dynamics when the gyroscopic effect is not considered. The only difference of the two systems is that the transverse and polar mass moment inertia are 8.46e-3 kg·m2 and 2.26e-4 kg·m2 for the long rotor, respectively, and 1.2e-3 kg·m2 and 4.3e-3 kg·m2 for the short rotor, respectively.

Figure 7 shows the root loci of the two systems. Initially, both systems have the same sets of quadruple

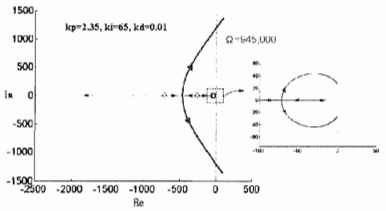

(a) Long rotor

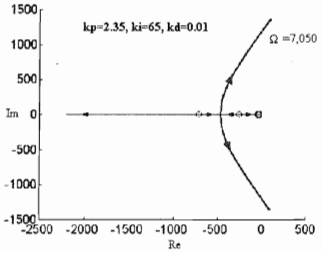

(b) Short rotor

Fig. 7 Root loci of the two systems

poles (-714, -261, -35.7). As the rotating speed increases, three pairs of poles will stay unchange and the other three pairs of poles become two single poles and two pairs of complex poles. Moreover, the systems will reach to marginally stable condition when the rotating speed increases to 945,000 rpm for the long rotor and 7,050 rpm for the short rotor. Obviously, the gyroscopic effect on the stability is more significant for the case of short shaft system. Let us further define δ to be the ratio of the polar mass moment inertia to the transverse mass moment inertia. Consequently, for the above long and short rotor systems the ratios are 2.67e-2 and 3.58, respectively, and the magnitudes of gyroscopic effect (α) from Ω=0 to 12,000 rpm are 0 to 16.8 and 0 to 2250, respectively. Figure 8 shows the relationship of the ratio δ and the maximum stable rotating speed. It is apparent that as the ratio δ increases, the maximum stable rotating speed will decrease.

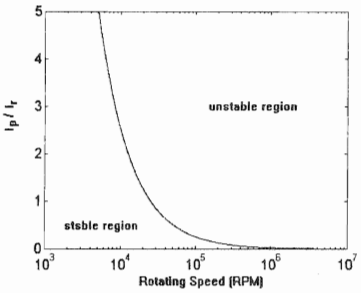

Fig. 8 Stability relationship between δ and the rotating speed

From the above study, we obtain that the gyroscopic effect cannot always be neglected especially for a short rotor system. As a matter of fact, the stability conditions can also be derived from equations (16) and (22) by Routh's stability criterion when the gyroscopic term is taken into account. However, the results obtained would become so complicated that it is unsuitable for the design purpose. Alternatively, we can design the decentralized PID controller by the following procedure. Given the maximum operating speeds, first determine the PID gains without considering the gyroscopic effect by pole assignment method so that the system's quadruple poles will be located at desired position. Then, check weather the system's poles at the maximum operating speed still satisfies the desired condition (e.g., over-damped condition) by equation (22). If so, the design procedure stop. Otherwise, move the quadruple poles further away from the image axis and redesign the new PID gains. For example, we wish to design the system to be an over-damped system with maximum operating speed 12,000 rpm. Assign the system poles at the neighborhood of -700, -250 and -30 for the long rotor system. By applying the above procedure, we obtain one of the solutions κ_p=2.35, κ_i=65 and κ_d=0.01 which make the system's quadruple poles be located at the position of -714, 261 and 35.7. The root loci are as same as that shown in Figure 7 (a) where at the maximum operating speed, the system poles are all in the negative real axis. When the rotating speed runs beyond 84,000 rpm, four poles will break away and become complex poles.

4. Experiment Results and Discussion

Figure 9 shows the photograph of the test rotor. The rotor consists of two sets of PEMBs, a driving motor, a hardened high carbon steel rigid shaft, two backup bearings, and a flexible coupling. The rated maximum rotating speed of the driving motor is 12,000 rpm and the coefficient k_d and k_i is designed to be 65000 N/m and 13 N/A, respectively.

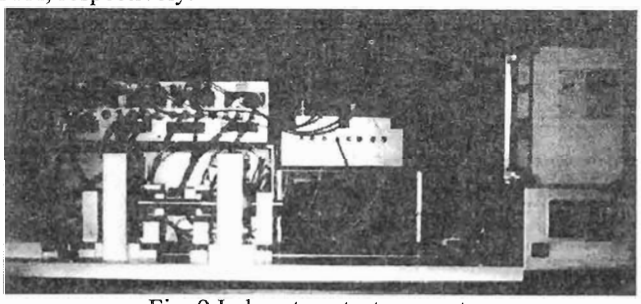

Fig. 9 Laboratory test apparatus

A bipolar linear current amplifier is developed for use in the PEMBs. Figures 10 and 11 show the circuit and the photograph of the bipolar linear current amplifier, respectively. The current amplifier is composed of the push-pull emitter follower circuit with current feedback signal.

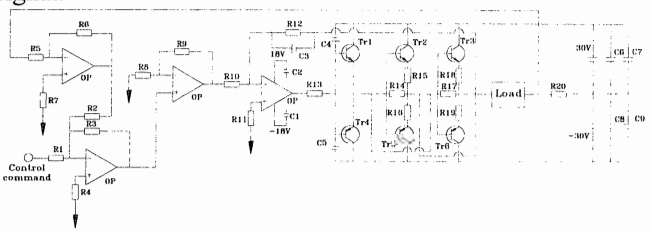

Fig. 10 Circuit of the bipolar linear current amplifier

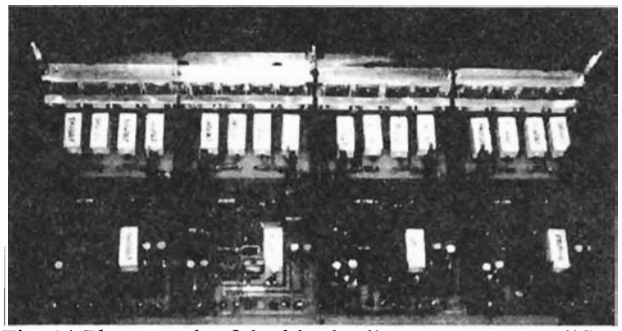

Fig. 11 Photograph of the bipolar linear current amplifier

In this study, we need four pieces of controller to control the system. Figure 12 shows the circuit and photograph of the controller. The four decentralized feedback PID gains are designed to be κ_p=2.35, κ_i=65 and κ_d=0.01. When rotating speed is 12,000 rpm, the corresponding eigenvalues are -714(double poles), -261(double poles), -35.7(double poles), -715, -713, -262, -260, -35.8, and -35.6. Figure 13 summarizes experimental results of the rotor orbits at low and high speeds. Figure 14 is the vibrational amplitude spectrum . The figures reveal that the rotor displacements are well controlled within an acceptable small range that the maximum vibration amplitude is no more than 30 μm.

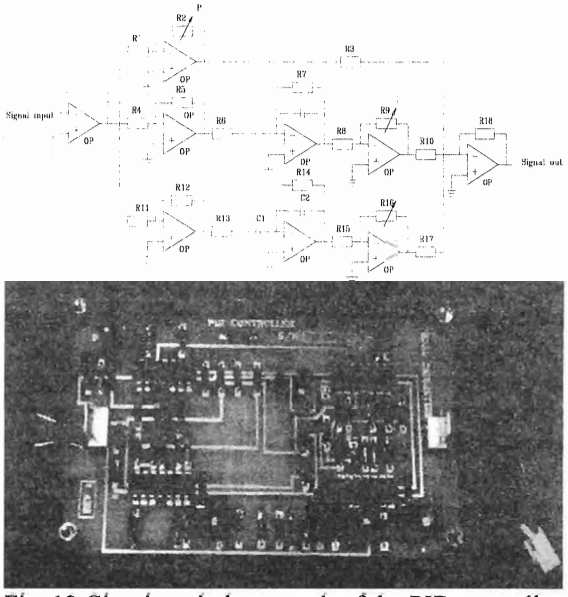

Fig. 12 Circuit and photograph of the PID controller

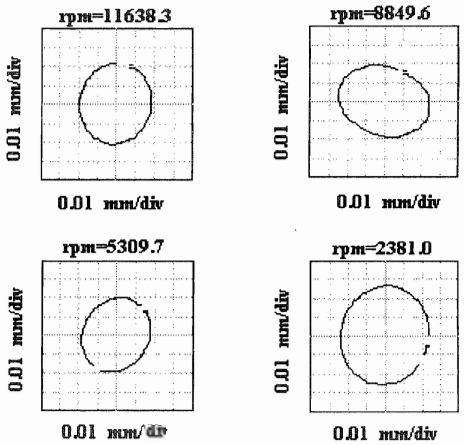

(a) Orbits at the right magnetic-bearing position

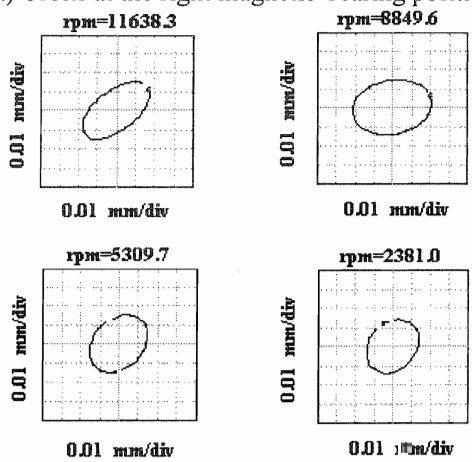

(b) Orbits at the left magnetic-bearing position

Fig. 13 Rotor orbits at low and high speeds

Figure 15 shows the impulse response of the free end, where an impulse force is applied at the middle point of the shaft at 0.04 sec in the negative direction of Y axis. The recover time is about 0.1 sec.

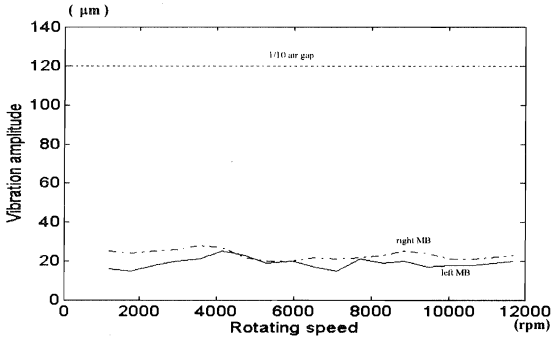

Fig. 14 The vibrational amplitude spectrum

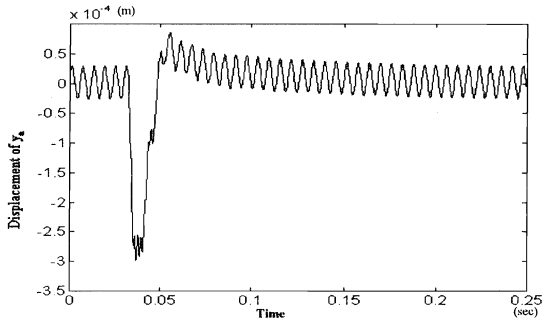

Fig. 15 Impulse response of y_b

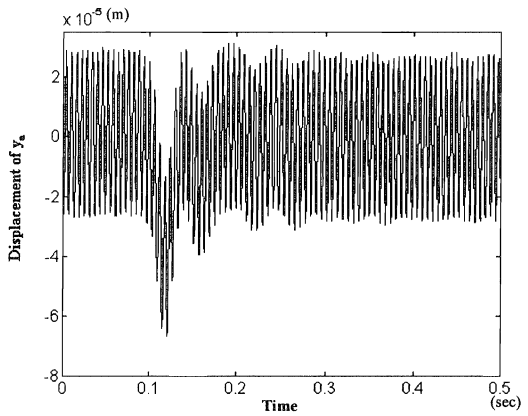

Fig. 16 Step response for the decentralized PID controller

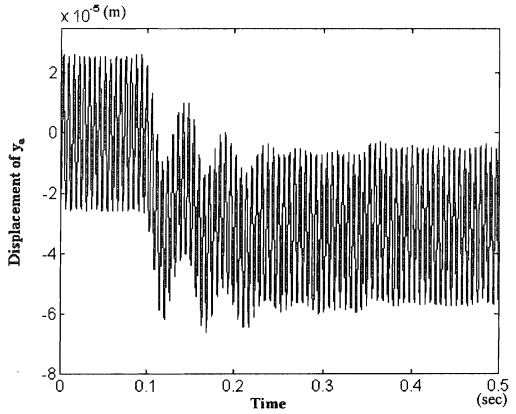

Fig. 17 Step response for the decentralized PD controller

Figure 16 and 17 show the step responses of the system controlled by decentralized PID and decentralized PD controller [7], respectively. Both cases have the same values of PD gains, and are all designed to be over-damped systems. The step force of about 2.5N is applied at 0.1 sec. Obviously, the case for the PID controller will soon return back to the desired point, but for PD controller, it always exists a constant deflection.

5. Conclusion

This study has presented a decentralized PID controller along with a semi-decentralized PID controller to stabilize the inherently unstable magnetic suspension system. Two types of rotor is adopted to demonstrate that it is sometimes unsuitable to design a decentralized PID controller without considering the gyroscopic effect, especially for a short rotor, such as turbine or flying wheel. Furthermore, the decentralized PID controller is implemented to a long rotor system. Experimental results show that the rotor system operates well at speed up to 12,000 rpm.

Acknowledgment- This study was supported by the National Science Council, Republic of China, under contract number NSC 84-2212-E-009-05.

References

[1] F. Matsumura, M. Kido, and Y. Tanaka, "Design Method of Horizontal Shaft Attractive Controlled Magnetic Bearing and Its Characteristics," Electrical Engineering in Japan, Vol. 103, No. 3, pp. 130-137, 1983.

[2] F. Matsumura, Y. Tanaka, and M. Kido, "Composition of a Magnetic-Bearing System for Horizontal Shaft and Its Experimental Results," Electrical Engineering in Japan, Vol. 103, No. 5, pp. 121-128, 1983.

[3] F. Matsumura, and T. Yoshimoto, "System Modeling and Control Design of a Horizontal-Shaft Magnetic-Bearing," IEEE Transactions on Magnetics, Vol. MAG-22, No. 3, PP. 196-203, 1986.

[4] D. C. Han, I. B. Jang, and S. C. Jung, "A Study on the PID Controlled Magnetic Bearing of a Rotor System," ASIA-Pacific Vibration Conference, Kitakyushu, pp. 1020-1025, November 1993.

[5] F. Matsumura, and H. Kobayashi, "Fundamental Equation for Horizontal Shaft magnetic Bearing and its Control System Design," Electrical Engineering in Japan, Vol. 101, NO. 3, pp. 123-130, 1981.

[6] H. Bleuler, and G. Schweitzer, "Dynamics of a Magnetically Suspended Rotor with Decentralized Control," Proc. IASTED Symp. Applied Control and Identification, Copenhagen, Denmark, pp. 19_17-19_22, June 1983.

[7] Yi-Hua Fan and An-Chen Lee, "Decentralized Control of a Rotor System Supported by Magnetic Bearings," International Journal of Machine Tools & Manufacture, Vol. 35, No. 3, pp. 445-458, 1995.

[8] A. C. Lee, F. Z. Hsiao, and D. Ko, "Analysis and Testing of a Magnetic Bearing with Permanent Magnets for Bias," JSME, Int. J. Ser. III, Vol. 37, No. 3, pp. 774-782, 1994.

[9] A. C. Lee, F. Z. Hsiao, and D. Ko, "Performance Limits of Permanent Magnet Biased Magnetic Bearings," JSME, Int. J. Ser. III, Vol. 37, No. 3, pp. 783-794, 1994.